

VIRO: Robust and Efficient Neuro-Symbolic Reasoning with Verification for Referring Expression Comprehension

Hyejin Park Junhyuk Kwon Suha Kwak Jungseul Ok[†]
 Pohang University of Science and Technology (POSTECH), South Korea
 {parkebbi2, treejkh, suha.kwak, jungseul}@postech.ac.kr

Abstract

Referring Expression Comprehension (REC) aims to localize the image region corresponding to a natural language query. Recent neuro-symbolic REC approaches leverage large language models (LLMs) and vision-language models (VLMs) to perform compositional reasoning, decomposing queries into structured programs and executing them step-by-step. While such approaches achieve interpretable reasoning and strong zero-shot generalization, they assume that intermediate reasoning steps are accurate. However, this assumption causes cascading errors: false detections and invalid relations propagate through the reasoning chain, yielding high-confidence false positives even when no target is present in the image. To address this limitation, we introduce Verification-Integrated Reasoning Operators (VIRO), a neuro-symbolic framework that embeds lightweight operator-level verifiers within reasoning steps. Each operator executes and validates its output, such as object existence or spatial relationships, allowing the system to robustly handle no-target cases through verification-aware abstention. Our framework achieves state-of-the-art performance, reaching 61.1% balanced accuracy across target-present and no-target settings, and demonstrates generalization to real-world egocentric data. VIRO also shows high reliability with a program failure rate of at most 0.3%, efficient per-query runtime, and scalability through decoupled program generation and execution. Code is available at <https://github.com/ml-postech/VIRO-neuro-symbolic-reasoning-with-verification>.

1. Introduction

Humans naturally interpret visual scenes through structured language, such as “the blue cup on the wooden table,” to identify objects through a sequence of semantic relations. This fundamental human skill is formalized in the vision-language task of Referring Expression Comprehen-

sion (REC), where the goal is to localize a target object in an image based on a natural language description [27]. This task has broad applicability, including vision-language navigation [35, 46], human-robot interaction [14, 32], and text-to-image retrieval [19].

Early REC approaches relied on supervised end-to-end models that directly map textual queries to image regions [15, 38, 44], which lack generalization. More recent work has moved toward compositional and LLM-driven reasoning, where a query is parsed into a program or sequence of modular operators for object detection, attribute filtering, and spatial reasoning [10, 31, 33]. These methods often build on open-vocabulary detectors (OVDs) [21, 25, 37] to align visual candidates with natural-language cues and generalize to unseen compositions [3, 4, 16, 34]. While improving interpretability, these methods still lack verification of intermediate reasoning steps.

In existing compositional pipelines, intermediate outputs, such as object proposals, attribute matches, and spatial relations, are typically assumed to be correct and are propagated without explicit checks. This leaves the system vulnerable to cascading errors, especially when OVDs produce high-confidence false positives for non-existent objects [22]. The problem is particularly severe in no-target cases, where pipelines are effectively forced to select one of these false positives as the answer. Moreover, many of these systems suffer from efficiency and scalability issues: (i) existing systems often place heavy multimodal LLMs in the inner loop, which leads to substantial latency, and (ii) program generation is tightly coupled with execution, often requiring regeneration of a separate program for each frame in a video, causing computational cost to grow linearly.

To address these challenges, we propose Verification-Integrated Reasoning Operators (VIRO), a neuro-symbolic framework that integrates verification at the operator level. Our pipeline first uses an LLM to translate a natural-language description into a sequence of executable operators, and then executes them sequentially, as illustrated in Figure 1. Each applicable operator not only performs a reasoning action but also validates its own result. These

[†]: corresponding author

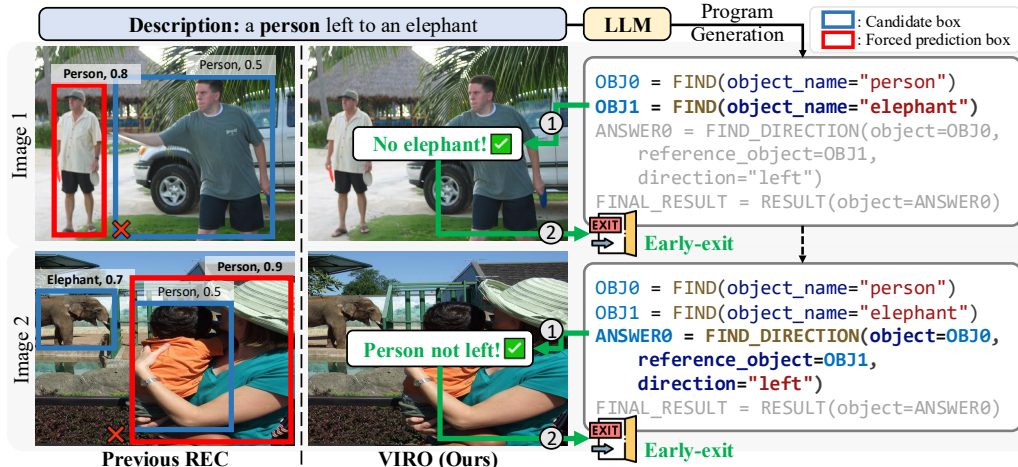


Figure 1. **Missing verification leads to forced predictions, which VIRO prevents.** Illustrative comparison between previous REC methods and our VIRO framework in no-target cases. Previous REC methods (left) are forced to output a prediction, even when the query cannot be grounded in the image, due to the lack of a mechanism for eliminating incorrect candidates. In contrast, our VIRO framework (right) terminates early instead of hallucinating a prediction: (i) `FIND` operator identifies that there is no elephant in the image (top); (ii) `FIND_DIRECTION` operator identifies the person is not positioned to the left of the elephant (bottom).

include uncertainty verification, where lightweight CLIP-based filters suppress high-confidence false positives from OVDs, and logical verification, which checks whether spatial and relational constraints are actually satisfied. When verification does not pass, indicating that no valid target exists, the operator abstains and triggers early termination, enabling explicit no-target detection.

We evaluate VIRO in a zero-shot setting on both no-target and standard REC scenarios. To highlight the importance of verification, we first demonstrate strong robustness on the gRefCOCO no-target dataset [11, 24], where images contain no instance matching the query. Furthermore, VIRO achieves state-of-the-art performance compared to compositional baselines on standard REC benchmarks, including RefCOCO+/g [26, 43] and the adversarial RefAdv dataset [1]. Beyond accuracy, VIRO achieves low program failure rates and efficient per-query runtime. By amortizing a single generated program across multiple images, it scales seamlessly to the 1-query- N -images setting, which we comprehensively validate on the egocentric RefEgo dataset [18]—a benchmark comprising both target-present and no-target frames.

Our key contributions are summarized as follows:

- We identify forced prediction as a fundamental failure mode of compositional vision-language reasoning, and introduce verification-integrated operators to address it.
- We design operator-level programs in which each operator both acts and verifies, using uncertainty- and logic-based checks to suppress error cascades and enable explicit no-target detection.
- In a zero-shot setting, VIRO demonstrates strong robustness on the gRefCOCO no-target split and achieves state-of-the-art performance among compositional baselines

on standard REC benchmarks. By decoupling program synthesis from execution and amortizing a single program over many images, VIRO scales favorably in the 1-query- N -image regime.

2. Related Work

Referring Expression Comprehension. Early end-to-end REC models [15, 38] achieve strong performance on seen domains but suffer under distribution shifts. To improve zero-shot generalization, recent work has moved toward first decomposing the textual description into *structured* semantic units and then aligning them with candidate proposals generated by Faster R-CNN [30], as in MATNet [44]. Building on this paradigm, ReCLIP [33] combines CLIP-based matching with rule-based spatial reasoning, SS-CLIP [10] aligns textual and visual triplets via structural similarity, GroundVLP [31] fuses heatmaps derived from vision-language pre-training models with proposals from an open-vocabulary detector, and FLORA [4] formalizes natural-language queries into a formal language for probabilistic matching. While these approaches enable zero-shot transfer, they remain inflexible when queries deviate from pre-defined forms, limiting their ability to handle diverse linguistic inputs.

Compositional Reasoning REC. Compositional approaches aim to provide more flexible reasoning than fixed structured pipelines by decomposing a query into interpretable operations. ViperGPT [34] demonstrates this idea by generating executable Python code, but its reliance on unconstrained free-form code generation often leads to non-runnable programs. To improve reliability, we follow operator-based generation frameworks similar to Vis-

Table 1. **Overview of VROs.** All operators are designed to return a set of verified bounding boxes or an empty set (\emptyset) if its condition is not satisfied. Additional operators are provided in Appendix A.1.

Operator	Input Arguments	Verification Module	Built-in Models
FIND	object_name	CLIP-based verifier	OVD, CLIP
PROPERTY	object, attribute	CLIP score	CLIP
RELATIVE_DEPTH	object, reference_object, criteria	Relative depth relation	DepthAnything

Prog [9], which restrict the program space to well-defined primitives. HYDRA [16] introduces iterative planning with a planner–reasoner loop, and NAVER [3] performs self-correcting inference over multiple reasoning states, with a final verification step to check whether the predicted target matches the query. However, these approaches rely heavily on large multimodal models, *e.g.*, BLIP-2 [20], InternVL2 [5], which offers limited protection against execution-time reasoning errors and incurs substantial overhead. Moreover, existing methods typically assume that a valid target always exists, often forcing a prediction even when no object actually matches the query. In contrast, our framework integrates lightweight verification at the operator level to robustly reject no-target cases.

3. Method

In Section 3.1, we formally define the REC problem, extended to handle no-target cases. Subsequently, we present the neuro-symbolic reasoning pipeline VIRO in Section 3.2.

3.1. Problem Formalization

REC aims to localize a region within an image I that corresponds to a given natural language query Q . Conventional REC assumes that the target object described by the query is always present in the image. This assumption does not hold in practical applications, such as a visual search system or a robot searching for an object in a building [41, 42, 46], where the target is frequently absent from most images. We formalize the output of the model as:

$$Y = \begin{cases} B, & \text{if a target exists in } I, \\ \emptyset, & \text{otherwise.} \end{cases} \quad (1)$$

Here, $B = (x, y, w, h) \in \mathbb{R}^4$ denotes a bounding box in pixel coordinates, where (x, y) represents the center coordinates of the box, and w, h are its width and height. The \emptyset denotes the absence of a target, *i.e.*, no object corresponding to the query Q is present in the image.

3.2. Verification-Integrated Reasoning Operators

To address the task defined above, VIRO employs a two-stage neuro-symbolic pipeline. As illustrated in Figure 2, the pipeline consists of two main stages: (i) a pre-execution stage that translates the query Q into a symbolic program P (detailed in Section 3.2.2), and (ii) a program execution stage that runs this program P on the image I to localize the

referent (detailed in Section 3.2.3). The program P is constructed using verification operators, with additional details on their functionality presented in the following section.

3.2.1. Verification Reasoning Operators (VROs)

We define a finite set of primitive operators, termed VROs and denoted by \mathcal{O} , which form the building blocks of our VIRO framework as summarized in Table 1. A program is represented as $P = (o_1, o_2, \dots, o_T)$, where $o_t \in \mathcal{O}$ and T denotes the number of program lines. Each operator in \mathcal{O} is designed not only to perform a reasoning step but also to self-verify execution: if its verification condition is not satisfied, the operator returns an empty set (\emptyset), enabling early termination of the entire pipeline.

We categorize these operators into four functional categories: (i) **Identification operators**, such as FIND and PROPERTY, which detect candidates and refine entities based on specified attributes; (ii) **Absolute spatial operators**, such as LOCATE, SIZE, ORDER, and ABSOLUTE_DEPTH, which reason about position and scale in absolute terms; (iii) **Relative spatial operators**, such as FIND_DIRECTION, FIND_NEAR, FIND_INSIDE, and RELATIVE_DEPTH, which capture spatial relationships between multiple entities; (iv) **Termination operator**, namely RESULT, which concludes the program by mapping the selected object into the answer space. Further details of each predefined operator, including their arguments, are provided in Table 1. To illustrate how the verification module works, we detail two key examples below.

Uncertainty Verification (UV) in FIND Operator. The FIND operator takes an argument `object_name`, a noun phrase l (*e.g.*, “guy”) in the query Q (*e.g.*, “A middle guy in red”). It invokes an OVD model D (*e.g.*, Grounding DINO [25]) on image I with label l to generate a (possibly empty) set of proposals, *i.e.*, $\{B_j\}_{j=1}^M \leftarrow D(I, l)$. While state-of-the-art OVDs offer powerful zero-shot grounding, they can yield high-confidence false positives (FPs) that are visually or semantically similar to l , which can propagate error through the reasoning pipeline, as shown in Figure 2.

To mitigate FP proposals, we integrate a lightweight CLIP-based verification module within the FIND operator. This module provides a secondary check on the OVD’s proposals by leveraging CLIP’s discriminative power of binary classification tasks, effectively filters uncertain outputs while adding minimal computational overhead. Specifically, for each proposal B_j , we crop its corresponding im-

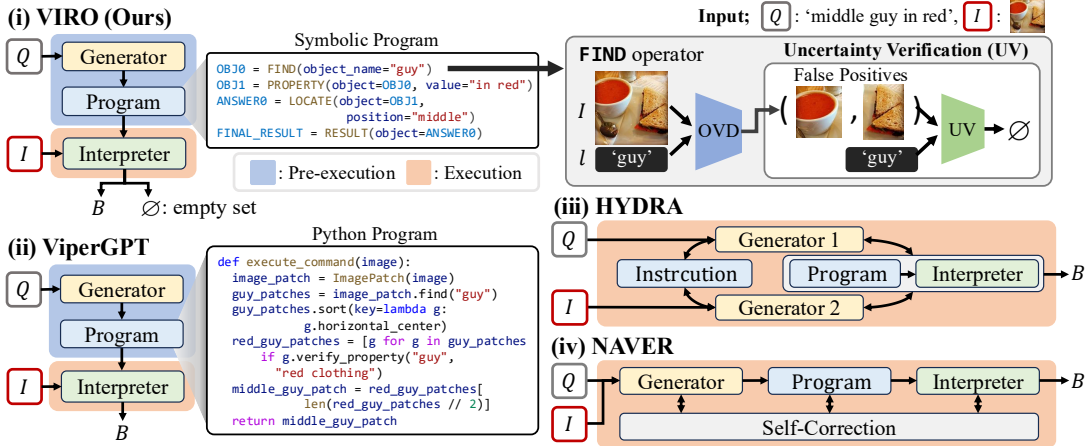


Figure 2. **VIRO vs. prior compositional REC.** (i) VIRO generates a symbolic program with an LLM, then an interpreter executes operators with *operator-level verification*; as exemplified by the `FIND` operator using CLIP-based uncertainty verification to prune OVD proposals. In contrast, (ii) ViperGPT compiles queries into Python code but lacks verification, while (iii) HYDRA and (iv) NAVER tightly couple program generation and execution, requiring iterative generators for all inputs.

age region, denoted as I_j . We predefine a bank of K common categories $\mathcal{C} = \{c_1, c_2, \dots, c_K\}$ that are well represented in CLIP and serve as negative anchors for verification, where K denotes the number of negative anchors. The verification score for B_j is the average probability of being the target l when compared one-on-one against each $c_k \in \mathcal{C}$:

$$S(l|I_j) = \frac{1}{K} \sum_{k=1}^K \frac{\exp(\text{sim}(I_j, l)/\tau)}{\exp(\text{sim}(I_j, l)/\tau) + \exp(\text{sim}(I_j, c_k)/\tau)}, \quad (2)$$

where $\text{sim}(\cdot, \cdot)$ denotes cosine similarity between CLIP image/text embeddings and $\tau > 0$ is a temperature. We accept B_j as l only if $S(l|I_j) \geq \delta_l$, where δ_l is a fixed or label-specific adaptive threshold. There is a trade-off in setting the threshold: when it is set close to 0.5, true positives (TP) may be filtered out, while FPs may remain unfiltered. Since CLIP can exhibit inherent bias toward labels that were well-represented in its training data, this can affect the accuracy of the thresholding process. To mitigate this, we use ImageNet [6] as an auxiliary dataset for per-label threshold calibration. Details of the calibration process are provided in Appendix A.1.3. To summarize, $S(l|I_j)$ serves as an uncertainty filter, assessing the degree of alignment between the given label l and the regions I_j proposed by OVD, and filtering out uncertain proposals.

Logical Verification (LV) in `FIND_DIRECTION` Operator. The `FIND_DIRECTION` operator takes three arguments: `object`, `reference_object`, and `direction`. `object` refers to the target object that we are trying to find, while the `reference_object` is the object used as a reference for comparison. It performs a

geometric test over all input candidates to verify whether each `object` proposal satisfies the specified spatial relation with respect to at least one `reference_object`.

3.2.2. Pre-execution Stage: Program Generation

The pre-execution stage translates a given natural-language query Q into a machine-executable symbolic program P , which is composed of our primitive operators defined in Section 3.2.1. This translation into a structured format is crucial for ensuring robust execution, as the inherent complexity of natural language makes direct machine interpretation unreliable. This process is accomplished through two key components: a program generator that produces an initial program, and a program validator that subsequently ensures its syntactic correctness.

Program Generation. We leverage a Large Language Model (LLM) to translate the natural language query Q into a symbolic program P . We guide this process using a few-shot prompting strategy as in [9], where the prompt contains a set of exemplars m demonstrating the desired query-to-program mapping:

$$P = \text{LLM}(Q|m) = (o_1, o_2, \dots, o_T), \text{ where } o_t \in \mathcal{O}. \quad (3)$$

Program Validation. LLMs can occasionally produce programs with syntactic errors such as malformed syntax, wrong operator names, or mismatched arguments. To mitigate this, we introduce a program validator that ensures strict conformance to our predefined operator-based grammar. Unlike ViperGPT’s open-ended Python code, which is prone to runtime or library-call errors, our approach restricts the output space to a symbolic structure.

If validation fails, a concise diagnostic feedback is provided to the LLM to trigger an immediate self-revision.

This structured validation loop, combined with our compact operator set, allows our symbolic approach to achieve significantly lower failure rates compared to existing methods, as evidenced in Section 4.2.2. Detailed diagnostic rules are provided in Appendix A.2.

3.2.3. Execution Stage: Program Interpretation

The program interpreter executes the symbolic program $P = (o_1, o_2, \dots, o_T)$ sequentially, invoking the corresponding operator at each step. Each operator relies on a built-in model to function properly, and we leverage the following models: GroundingDINO [25] or GLIP [21], CLIP [28], and DepthAnything [40]. Execution continues until either (i) all operators are applied and RESULT maps the final candidates to an answer box, or (ii) some operator returns \emptyset , yielding a no-target outcome for the current image and immediately terminating execution. The latter corresponds to an early-exit, which occurs when built-in verification rejects all proposals (e.g., FIND identifies there is no valid object; FIND_DIRECTION finds no relation). This mechanism enables explicit no-target handling and reduces unnecessary computation, as demonstrated in Section 4.3, thereby highlighting the robustness of our verification-integrated design.

3.2.4. Decoupled Neuro-Symbolic Approach

As shown in Figure 2, VIRO adopts a decoupled design that separates program generation from execution. In contrast, methods such as HYDRA [16] and NAVER [3] entangle program synthesis for a query Q with image execution. Consequently, even when the query is identical across N images, these systems regenerate a reasoning program for each image I_i , incurring N separate synthesis operations. VIRO generates the program once and reuses it across all images, enabling low-latency operation. Empirical results are reported in Section 4.2.2.

4. Experiment

In this section, we present a comprehensive evaluation of our VIRO pipeline. The details of the experimental setup are described in Section 4.1. We then present our main results in terms of robustness, efficiency, and scalability in Section 4.2. Following this, we conduct extensive ablation studies in Section 4.3.

4.1. Experimental Setup

Implementation Details. We primarily follow the official implementations of each baseline, using their default hyperparameter settings. Unless otherwise noted, detection thresholds for open-vocabulary detectors are fixed based on validation performance on RefCOCO. For all program generation, we use Qwen2.5-72B-Instruct-AWQ [39], known for strong code-generation, to ensure a fair comparison with Python-code baselines such as ViperGPT.

Dataset and Evaluation Metrics. We evaluate our framework on both no-target scenarios and standard benchmarks. For the no-target setting, we use the gRefCOCO dataset [11] no-target split, which contains referring expressions that do not correspond to any object in the image. This setting allows us to directly evaluate the model’s ability to suppress incorrect predictions in the absence of a valid target. For standard REC, we evaluate our method on widely used REC benchmarks, including RefCOCO/+ [43], and RefCOCOg [26]. We further assess the consistency of linguistic structure comprehension on RefAdv [1], and extend evaluation to the video domain with RefEgo [18], which includes both target-present and no-target cases. We further show that VIRO can be modularly extended to GQA [12], suggesting potential applicability beyond REC, with detailed results provided in Appendix A.10.

We evaluate both no-target robustness and standard REC accuracy via **Balanced Accuracy**, defined as $(\text{TPR} + \text{TNR})/2$. It provides a holistic measure by equally weighing the ability to localize existing targets and reject non-existing ones. The component metrics are defined as follows:

- **True Positive Rate (TPR)** = $\frac{TP}{TP+FN}$, measuring accuracy on target-present samples. This is equivalent to the standard Acc@0.5, used in standard REC, where a prediction is correct if IoU between the predicted and ground-truth bounding boxes exceeds 0.5.
- **True Negative Rate (TNR)** = $\frac{TN}{TN+FP}$, measuring accuracy on target-absent samples, often referred to as no-target accuracy (N-acc).

Baselines. We group existing REC approaches into four categories, according to their underlying assumptions. **Fully supervised REC** includes methods trained with full annotations on RefCOCO+/g, while GREC [11] additionally uses no-target supervision to handle target-absent cases. **Proposal-based REC** methods first parse the referring expression to extract key linguistic components and then align them with candidate region proposals. Such approaches inherently force the model to select one of the proposals, which makes handling no-target cases intrinsically difficult. **Detector-based REC** leverages large-scale pretrained grounding detectors to directly match textual phrases with image regions in an end-to-end manner, without explicit proposal ranking. For this category, we select GroundingDINO-T [25] and GLIP-L [21] as representative methods. Importantly, neither model was trained on the MSCOCO captions underlying our evaluation benchmarks; accordingly, we evaluate them in a zero-shot setting to ensure a fair comparison. Finally, **compositional reasoning REC**, which serves as our primary point of comparison, explicitly parses and executes the linguistic structure to localize referents through multi-step reasoning. More explanations of the baselines and additional details of the experimental setup are provided in Appendix A.3.

Table 2. Comparison of REC methods on no-target robustness using gRefCOCO no-target and standard REC performance using RefCOCO across the TestA and TestB splits. For each split, we report **Balanced Accuracy** (Bal. Acc.), along with its component metrics **True Negative Rate** (TNR; N-acc), and **True Positive Rate** (TPR; Acc@0.5).

Method	TestA			TestB		
	Bal. Acc. \uparrow	TNR (gRef) \uparrow	TPR (Ref) \uparrow	Bal. Acc. \uparrow	TNR (gRef) \uparrow	TPR (Ref) \uparrow
Fully Supervised REC [11]						
Qwen2.5-VL-72B-AWQ [†] [2]	69.5	47.3	91.7	66.8	45.1	88.4
GREC-MDETR-R101 [15]	62.0	34.5	89.6	56.2	31.0	81.4
GREC-UNINEXT-R50 [38]	70.4	49.3	91.5	67.6	48.2	86.9
Proposal-based REC						
ReCLIP [33]	23.5	0.0	47.0	22.6	0.0	45.2
SS-CLIP [10]	33.3	0.0	66.5	27.5	0.0	54.9
GroundVLP [31]	30.7	0.0	61.3	21.8	0.0	43.5
Detector-based REC						
GLIP-L [21]	37.2	21.7	52.6	30.0	18.2	41.8
GroundingDINO-T [25]	40.0	22.8	57.2	29.6	16.0	43.2
Compositional Reasoning REC with GroundingDINO						
ViperGPT [34]	33.4	0.2	66.7	27.4	0.1	54.6
HYDRA [16]	35.2	7.5	62.8	34.7	7.0	62.4
NAVER [3]	33.8	3.4	64.2	30.0	1.8	58.2
VIRO (Ours)	61.1	50.2	71.9	56.9	52.9	60.8

Note: [†]We append a negative instruction, e.g., “If there is no object, return []”. Without this prompt, the model struggles to detect no-target cases, reducing TNR 3.1% (TPR 94.7%) on TestA.

4.2. Main Results

We evaluate our framework along three key dimensions: (i) robustness in handling *no-target* cases (Section 4.2.1), (ii) efficiency in terms of failure rate and execution latency (Section 4.2.2), and (iii) scalability, highlighting the benefits of our decoupled pipeline (Section 4.2.3). Furthermore, we extend our evaluation to a real-world egocentric setting with the RefEgo dataset, which includes both target-present and no-target cases (Section 4.2.4).

4.2.1. Robustness on No-Target Cases

Table 2 reports results on the RefCOCO TestA and TestB splits, where TestA contains person referents and TestB contains object-centric referents. The proposal-based baselines yield near-zero TNR because they operate as forced-prediction systems, selecting one region from a pre-generated proposal pool (e.g., Faster R-CNN in MatNet [30, 44]) whenever candidate boxes are available. Similarly, lacking abstention mechanisms, detector-based and compositional REC methods often select hallucinated OVD detections. This forced-prediction setup introduces an implicit trade-off: under target-present assumptions, such methods may appear stronger than in no-target-aware settings. We revisit this point in Appendix A.4, showing that our method also attains higher TPR when abstention is disallowed. Since baseline models inherently lack no-target handling, the criteria we established to evaluate their no-target cases are detailed in Appendix A.5.

In contrast, VIRO achieves 61.1% and 56.9% Balanced Accuracy on TestA and TestB, respectively, substantially outperforming all compositional reasoning baselines with-

out REC fine-tuning. These gains stem from verification-integrated operators that enable abstention when no valid referent is present. Crucially, VIRO remains competitive with fully supervised methods (e.g., GREC-UNINEXT) despite not using no-target annotations, demonstrating robust zero-shot visual grounding. Results on the remaining splits are provided in Appendix A.6.

4.2.2. Efficiency of Compositional Reasoning on Standard REC Benchmarks

Table 3 compares VIRO with compositional reasoning REC baselines on standard REC benchmarks in terms of accuracy, program failure rate (FR), and runtime efficiency. Due to space constraints, RefAdv results for linguistic understanding are reported in Appendix A.6.4. To rigorously assess reliability, the inclusive accuracy (Inc.) strictly penalizes program failures as incorrect predictions [3]. VIRO exhibits a remarkably low program failure rate of less than 0.3%, making its Inc. and Exc. accuracies nearly identical. In contrast, HYDRA and NAVER frequently fail due to syntactically invalid LLM-generated programs or execution timeouts when no answer is found within their default iteration budgets (7 and 5, respectively). VIRO’s integrated validator, with a maximum of 5 iterations, ensures that nearly all generated programs are executable, overcoming a critical bottleneck of previous compositional approaches.

Moreover, VIRO incurs lower execution runtime (Exec.), indicating that its structured operator-based reasoning introduces little additional computational overhead. This makes VIRO well suited for large-scale image processing per query, as analyzed in the following section. Details

Table 3. Comparison of compositional reasoning accuracy and efficiency on REC benchmarks. All results are evaluated using Qwen2.5-72B-Instruct-AWQ on RefCOCO/RefCOCO+ (testA) and RefCOCOg (test). TPR (Acc@0.5) is measured both including (Inc.↑) and excluding (Exc.↑) failure cases and FR denotes the Failure Rate (%). Runtime (query/s) is measured on the RefCOCO testA split using an NVIDIA RTX A6000 GPU; E2E refers to total per-query latency, while Exec. refers to the execution-stage only.

Method	RefCOCO			RefCOCO+			RefCOCOg			E2E ↓	Exec. ↓
	FR ↓	Exc.↑	Inc.↑	FR ↓	Exc.↑	Inc.↑	FR ↓	Exc.↑	Inc.↑		
Fully Supervised REC											
Qwen2.5-VL-72B-AWQ [2]	0.12	94.4	94.3	0.17	91.8	91.6	0.11	89.1	89.0	9.39	9.39
Detector-based REC											
GLIP-L [21]	0.00	52.6	52.6	0.00	48.6	48.6	0.00	52.6	52.6	0.81	0.81
GroundingDINO-T [25]	0.00	57.2	57.2	0.00	57.6	57.6	0.00	59.5	59.5	0.20	0.20
Compositional Reasoning REC with GroundingDINO											
ViperGPT [34]	3.45	66.7	64.4	6.83	61.7	57.5	6.03	65.7	61.7	30.19	1.49
HYDRA [16]	28.46	62.8	44.9	35.96	58.4	37.4	32.37	67.1	45.4	37.06	30.57
NAVER [3]	6.01	64.2	60.3	7.39	60.1	55.6	9.74	68.4	55.8	7.74	7.08
VIRO (Ours)	0.07	71.9	71.9	0.00	63.3	63.3	0.30	66.6	66.3	12.92	0.71

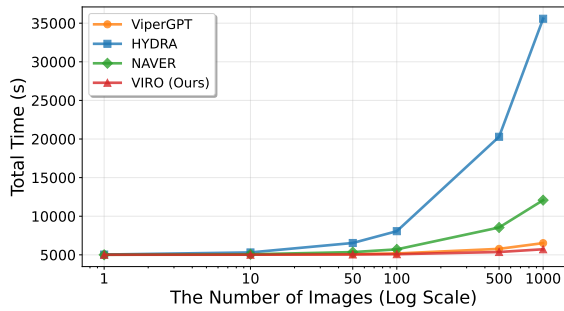


Figure 3. Total inference time (s) in a 1-query- N -images setting, with the x -axis on a logarithmic scale.

regarding pre-execution acceleration via API-based LLMs (e.g., GPT-4o/mini [13]) and baseline VRAM requirements are provided in Appendices A.7 and A.8, respectively.

4.2.3. Scalability in 1-Query- N -Images

We evaluate the scalability of VIRO in a 1-query- N -images setting—a crucial scenario for real-world applications like robotic visual search. As shown in Figure 3, VIRO and ViperGPT demonstrate exceptional scalability. Due to its decoupled architecture, the program generation is performed only once per query, i.e., $T_{\text{total}} = T_{\text{pre-execution}} + N \times T_{\text{execution}}$. In contrast, entangled methods like HYDRA and NAVER force program regeneration for each image, i.e., $T_{\text{total}} = N \times T_{\text{pre-execution}} + N \times T_{\text{execution}}$. This severe computational overhead makes them impractical for large-scale tasks, highlighting the critical advantage of our decoupled design for low-latency visual reasoning.

4.2.4. Robustness Evaluation on RefEgo

RefEgo [18] is a video-based REC benchmark built upon Ego4D [8], designed to evaluate grounding under egocentric motion and varying target visibility. Unlike static-image REC datasets, each video clip contains both target-present and no-target frames, requiring robust absent-target detec-

Table 4. Comparison of video-based REC performance on the RefEgo test set. Refer to Appendix A.6.5 for the corresponding validation set results.

Method	All Frames		Target-present
	mSTIoU	Acc@0.5+n	TPR (Acc@0.5)
Fully Supervised with RefEgo			
MDETR+BH [18]	36.9	51.1	53.0
Off-the-shelf RefCOCOg model			
OFA [36]	15.4	29.3	27.1
MDETR [15]	15.4	26.4	22.8
Compositional Reasoning REC with GroundingDINO			
ViperGPT [34]	13.0	23.0	27.6
VIRO (Ours)	22.8	51.9	36.2

tion. Since this setting naturally corresponds to the 1-query- N -images scenario (Section 4.2.3), we restrict our comparison to methods whose pre-execution is decoupled from execution. Following RefEgo, we report mean Spatio-Temporal IoU (mSTIoU) and ACC@0.5+n. For a video clip with N frames, STIoU is calculated as:

$$\text{STIoU} = \frac{\sum_{i=1}^N |p_i \cap t_i|}{\sum_{i=1}^N |p_i \cup t_i|}, \quad (4)$$

where p_i and t_i denote the predicted and ground-truth regions for frame i . The final mSTIoU is obtained by averaging STIoU across all test clips. For ACC@0.5+n, a frame contributes a score of 1 if its IoU exceeds 0.5 (target-present), or if correctly classified as no-target.

We compare VIRO against two types of baselines: (i) the fully supervised video REC model MDETR+BH trained on RefEgo, and (ii) off-the-shelf RefCOCOg-trained OFA [36] and MDETR [15] following the RefEgo setup. As shown in Table 4, VIRO demonstrates strong zero-shot capabilities. In the all-frames setting, including both target-present and no-target frames, VIRO attains competitive mSTIoU

Table 5. Ablation study of the proposed verification components in VIRO on the gRefCOCO no-target and RefCOCO testA dataset. ‘Fixed’ refers to a fixed threshold, while ‘adaptive’ refers to an adaptive threshold.

Method	Balanced Acc. \uparrow	No Target Robustness		Standard REC
		TNR (N-acc) \uparrow	TPR (Acc@0.5) \uparrow	TPR (Acc@0.5) \uparrow
Detector-only	40.0	22.8		57.1
+ Operators	56.8	38.9		74.6
+ LV	57.0	39.3		74.6
+ UV, fixed	58.8	43.1		74.4
+ UV, adaptive	61.1	50.2		71.9

and surpasses the fully supervised method in ACC@0.5+n. Furthermore, it yields the highest performance among zero-shot methods on target-present frames, confirming its robust grounding ability without domain-specific training.

4.3. Ablation Studies

In this section, we conduct ablation studies to analyze the impact of key hyperparameters on VIRO’s performance and to validate our design choices. Unless stated otherwise, all experiments are conducted using VIRO with GroundingDINO-T on the RefCOCO testA split. Additional ablations, including analyses of the LLM backbones (llama3.1-Instruct [7], GPT-4o/mini [13]) and the early-exit mechanism, are provided in Appendix A.9. Furthermore, qualitative results and execution examples of our pipeline are detailed in Appendices A.11 and A.12, respectively.

Verification Components. Table 5 shows the results of a cumulative ablation study to analyze the contribution of each verification module of our VIRO pipeline. We start with a standard detector-only baseline and progressively add our proposed modules to measure the impact on both no-target robustness and standard REC accuracy. Incorporating operators (without verification) boosts balanced accuracy to 56.8%, suggesting that the compositional pipeline effectively grounds all query noun phrases. Adding LV and UV further enhances no-target robustness, albeit with a slight TPR reduction reflecting a precision–recall trade-off.

OVD Detection Threshold. The detection threshold of the Open-Vocabulary Detector (OVD) is a critical parameter that governs the trade-off between standard REC accuracy (TPR) and no-target robustness (TNR). As shown in Figure 4, a higher threshold improves TNR by filtering out spurious detections, but this simultaneously lowers recall, which in turn degrades TPR. We adopt a threshold of 0.2 to favor high recall at the proposal stage while maintaining balanced overall performance.

CLIP Models. We analyze the impact of the CLIP model backbone, used for both UV and the PROPERTY operator. Table 6 compares the performance of ViT-L/14 and ViT-H/14. Our final configuration uses ViT-H/14 for its optimal

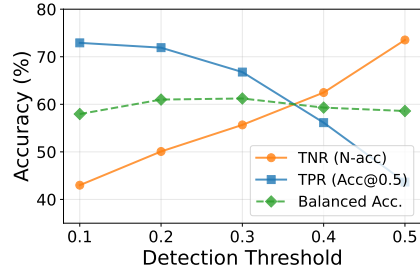


Figure 4. Analysis of the OVD detection threshold, illustrating the trade-off between TPR and TNR.

balance between accuracy and efficiency, while the lighter ViT-L/14 remains a computationally efficient alternative.

Table 6. Ablation on the CLIP backbone, comparing the trade-off between TPR and execution-stage (Exec.) runtime.

CLIP Model	TPR (Acc@0.5) \uparrow	Exec. \downarrow
ViT-H/14	71.9	0.71
ViT-L/14	68.8	0.55

5. Discussion and Conclusion

In this work, we introduced VIRO, a verification-integrated neuro-symbolic pipeline for REC. By embedding lightweight verification mechanisms at each reasoning step, our framework explicitly handles no-target scenarios, supports interpretable early termination, and maintains state-of-the-art accuracy with efficient execution and favorable scalability. Beyond REC, the modularity of our pipeline suggests promising extensions to interactive domains. In particular, the ability to parse natural language into verifiable symbolic programs opens the door to future applications where robots and humans engage in dialogue. In such scenarios, robots could not only interpret complex instructions but also execute them safely and transparently, ensuring that ambiguous commands are rejected before action. This direction underscores the broader potential of our approach as a foundation for trustworthy multimodal reasoning in embodied AI systems.

Acknowledgements. This work was supported by Institute of Information & Communications Technology Planning & Evaluation (IITP) grants funded by the Korea government (MSIT) (RS-2019-II191906, Artificial Intelligence Graduate School Program (POSTECH); RS-2024-00457882, AI Research Hub Project; IITP-2026-RS-2024-00437866, Information Technology Research Center (ITRC)). It was also supported by the Korea Institute for Advancement of Technology (KIAT) grant funded by the Ministry of Trade, Industry and Energy (MOTIE) (RS-2025-00564342), and the Seoul R&BD Program (SP240008) through the Seoul Business Agency (SBA) funded by the Seoul Metropolitan Government.

References

- [1] Arjun Akula, Spandana Gella, Yaser Al-Onaizan, Song-Chun Zhu, and Siva Reddy. Words aren't enough, their order matters: On the robustness of grounding visual referring expressions. In *Proceedings of the 58th Annual Meeting of the Association for Computational Linguistics*, pages 6555–6565, 2020. [2](#), [5](#), [13](#)
- [2] Shuai Bai, Keqin Chen, Xuejing Liu, Jialin Wang, Wenbin Ge, Sibao Song, Kai Dang, Peng Wang, Shijie Wang, Jun Tang, et al. Qwen2.5-vl technical report. *arXiv preprint arXiv:2502.13923*, 2025. [6](#), [7](#), [13](#), [14](#)
- [3] Zhixi Cai, Fucui Ke, Simindokht Jahangard, Maria Garcia de la Banda, Reza Haffari, Peter J. Stuckey, and Hamid Rezatofighi. Naver: A neuro-symbolic compositional automaton for visual grounding with explicit logic reasoning. In *Proceedings of the IEEE/CVF International Conference on Computer Vision*, 2025. [1](#), [3](#), [5](#), [6](#), [7](#), [14](#), [15](#), [16](#), [17](#), [18](#), [19](#)
- [4] Zhe Chen and Zijing Chen. Flora: Formal language model enables robust training-free zero-shot object referring analysis. *arXiv preprint arXiv:2501.09887*, 2025. [1](#), [2](#), [14](#)
- [5] Zhe Chen, Weiyun Wang, Hao Tian, Shenglong Ye, Zhangwei Gao, Erfei Cui, Wenwen Tong, Kongzhi Hu, Jiapeng Luo, Zheng Ma, et al. How far are we to gpt-4v? closing the gap to commercial multimodal models with open-source suites. *Science China Information Sciences*, 67(12):220101, 2024. [3](#), [15](#), [19](#)
- [6] Jia Deng, Wei Dong, Richard Socher, Li-Jia Li, Kai Li, and Li Fei-Fei. Imagenet: A large-scale hierarchical image database. In *2009 IEEE conference on computer vision and pattern recognition*, pages 248–255. Ieee, 2009. [4](#)
- [7] Aaron Grattafiori, Abhimanyu Dubey, Abhinav Jauhri, Abhinav Pandey, Abhishek Kadian, Ahmad Al-Dahle, Aiesha Letman, Akhil Mathur, Alan Schelten, Alex Vaughan, et al. The llama 3 herd of models. *arXiv preprint arXiv:2407.21783*, 2024. [8](#), [19](#)
- [8] Kristen Grauman, Andrew Westbury, Eugene Byrne, Zachary Chavis, Antonino Furnari, Rohit Girdhar, Jackson Hamburger, Hao Jiang, Miao Liu, Xingyu Liu, et al. Ego4d: Around the world in 3,000 hours of egocentric video. In *Proceedings of the IEEE/CVF Conference on Computer Vision and Pattern Recognition*, pages 18995–19012, 2022. [7](#), [13](#)
- [9] Tanmay Gupta and Aniruddha Kembhavi. Visual programming: Compositional visual reasoning without training. In *Proceedings of the IEEE/CVF Conference on Computer Vision and Pattern Recognition*, pages 14953–14962, 2023. [3](#), [4](#)
- [10] Zeyu Han, Fangrui Zhu, Qianru Lao, and Huaizu Jiang. Zero-shot referring expression comprehension via structural similarity between images and captions. In *Proceedings of the IEEE/CVF Conference on Computer Vision and Pattern Recognition*, pages 14364–14374, 2024. [1](#), [2](#), [6](#), [14](#)
- [11] Shuting He, Henghui Ding, Chang Liu, and Xudong Jiang. Grec: Generalized referring expression comprehension. *arXiv preprint arXiv:2308.16182*, 2023. [2](#), [5](#), [6](#), [13](#)
- [12] Drew A Hudson and Christopher D Manning. Gqa: A new dataset for real-world visual reasoning and compositional question answering. In *Proceedings of the IEEE/CVF Conference on Computer Vision and Pattern Recognition*, pages 6700–6709, 2019. [5](#), [20](#)
- [13] Aaron Hurst, Adam Lerer, Adam P Goucher, Adam Perelman, Aditya Ramesh, Aidan Clark, AJ Ostrow, Akila Welihinda, Alan Hayes, Alec Radford, et al. Gpt-4o system card. *arXiv preprint arXiv:2410.21276*, 2024. [7](#), [8](#), [19](#)
- [14] Tianlei Jin, Qiwei Meng, Gege Zhang, Qiulan Huang, Fangtai Guo, Shu Kong, Wei Song, Jiakai Zhu, and Jason Gu. Referring expression comprehension in semi-structured human–robot interaction. *Expert Systems with Applications*, 275:126965, 2025. [1](#)
- [15] Aishwarya Kamath, Mannat Singh, Yann LeCun, Gabriel Synnaeve, Ishan Misra, and Nicolas Carion. Mdetr-modulated detection for end-to-end multi-modal understanding. In *Proceedings of the IEEE/CVF International Conference on Computer Vision*, pages 1780–1790, 2021. [1](#), [2](#), [6](#), [7](#), [14](#), [15](#), [18](#)
- [16] Fucui Ke, Zhixi Cai, Simindokht Jahangard, Weiqing Wang, Pari Delir Haghighi, and Hamid Rezatofighi. Hydra: A hyper agent for dynamic compositional visual reasoning. In *European Conference on Computer Vision*, pages 132–149. Springer, 2024. [1](#), [3](#), [5](#), [6](#), [7](#), [14](#), [15](#), [16](#), [17](#), [18](#), [19](#)
- [17] Alexander Kirillov, Eric Mintun, Nikhila Ravi, Hanzi Mao, Chloe Rolland, Laura Gustafson, Tete Xiao, Spencer Whitehead, Alexander C Berg, Wan-Yen Lo, et al. Segment anything. In *Proceedings of the IEEE/CVF International Conference on Computer Vision*, pages 4015–4026, 2023. [18](#), [19](#)
- [18] Shuhei Kurita, Naoki Katsura, and Eri Onami. Refego: Referring expression comprehension dataset from first-person perception of ego4d. In *Proceedings of the IEEE/CVF International Conference on Computer Vision*, pages 15214–15224, 2023. [2](#), [5](#), [7](#), [13](#), [18](#)
- [19] Saehyung Lee, Sangwon Yu, Junsung Park, Jihun Yi, and Sungroh Yoon. Interactive text-to-image retrieval with large language models: A plug-and-play approach. In *Proceedings of the 62nd Annual Meeting of the Association for Computational Linguistics (Volume 1: Long Papers)*, pages 791–809, 2024. [1](#)
- [20] Junnan Li, Dongxu Li, Silvio Savarese, and Steven Hoi. Blip-2: Bootstrapping language-image pre-training with frozen image encoders and large language models. In *International Conference on Machine Learning*, pages 19730–19742. PMLR, 2023. [3](#), [19](#)
- [21] Liunian Harold Li, Pengchuan Zhang, Haotian Zhang, Jianwei Yang, Chunyuan Li, Yiwu Zhong, Lijuan Wang, Lu Yuan, Lei Zhang, Jenq-Neng Hwang, et al. Grounded language-image pre-training. In *Proceedings of the IEEE/CVF Conference on Computer Vision and Pattern Recognition*, pages 10965–10975, 2022. [1](#), [5](#), [6](#), [7](#), [14](#), [15](#), [16](#), [17](#), [18](#), [19](#)
- [22] Yifan Li, Yifan Du, Kun Zhou, Jinpeng Wang, Wayne Xin Zhao, and Ji-Rong Wen. Evaluating object hallucination in large vision-language models. In *Proceedings of the 2023 Conference on Empirical Methods in Natural Language Processing*, pages 292–305, 2023. [1](#)

- [23] Tsung-Yi Lin, Michael Maire, Serge Belongie, James Hays, Pietro Perona, Deva Ramanan, Piotr Dollár, and C. Lawrence Zitnick. Microsoft coco: Common objects in context. In *European Conference on Computer Vision*, pages 740–755. Springer, 2014. 13
- [24] Chang Liu, Henghui Ding, and Xudong Jiang. Gres: Generalized referring expression segmentation. In *Proceedings of the IEEE/CVF Conference on Computer Vision and Pattern Recognition*, pages 23592–23601, 2023. 2, 13
- [25] Shilong Liu, Zhaoyang Zeng, Tianhe Ren, Feng Li, Hao Zhang, Jie Yang, Qing Jiang, Chunyuan Li, Jianwei Yang, Hang Su, et al. Grounding dino: Marrying dino with grounded pre-training for open-set object detection. In *European Conference on Computer Vision*, pages 38–55. Springer, 2024. 1, 3, 5, 6, 7, 14, 15, 16, 17, 18, 19
- [26] Junhua Mao, Jonathan Huang, Alexander Toshev, Oana Camburu, Alan L Yuille, and Kevin Murphy. Generation and comprehension of unambiguous object descriptions. In *Proceedings of the IEEE Conference on Computer Vision and Pattern Recognition*, pages 11–20, 2016. 2, 5, 13
- [27] Yanyuan Qiao, Chaorui Deng, and Qi Wu. Referring expression comprehension: A survey of methods and datasets. *IEEE Transactions on Multimedia*, 23:4426–4440, 2020. 1
- [28] Alec Radford, Jong Wook Kim, Chris Hallacy, Aditya Ramesh, Gabriel Goh, Sandhini Agarwal, Girish Sastry, Amanda Askell, Pamela Mishkin, Jack Clark, et al. Learning transferable visual models from natural language supervision. In *International Conference on Machine Learning*, pages 8748–8763. PMLR, 2021. 5, 19
- [29] René Ranftl, Alexey Bochkovskiy, and Vladlen Koltun. Vision transformers for dense prediction. In *Proceedings of the IEEE/CVF International Conference on Computer Vision*, pages 12179–12188, 2021. 19
- [30] Shaoqing Ren, Kaiming He, Ross Girshick, and Jian Sun. Faster r-cnn: Towards real-time object detection with region proposal networks. *IEEE Transactions on Pattern Analysis and Machine Intelligence*, 39(6):1137–1149, 2016. 2, 6
- [31] Haozhan Shen, Tiancheng Zhao, Mingwei Zhu, and Jianwei Yin. Groundvlp: Harnessing zero-shot visual grounding from vision-language pre-training and open-vocabulary object detection. In *Proceedings of the AAAI Conference on Artificial Intelligence*, pages 4766–4775, 2024. 1, 2, 6, 14
- [32] Mohit Shridhar, Lucas Manuelli, and Dieter Fox. Cliport: What and where pathways for robotic manipulation. In *Conference on Robot Learning*, pages 894–906. PMLR, 2022. 1
- [33] Sanjay Subramanian, William Merrill, Trevor Darrell, Matt Gardner, Sameer Singh, and Anna Rohrbach. Reclip: A strong zero-shot baseline for referring expression comprehension. In *Proceedings of the 60th Annual Meeting of the Association for Computational Linguistics (Volume 1: Long Papers)*, pages 5198–5215, 2022. 1, 2, 6, 14
- [34] Dádac Surís, Sachit Menon, and Carl Vondrick. Vipergpt: Visual inference via python execution for reasoning. In *Proceedings of the IEEE/CVF International Conference on Computer Vision*, pages 11888–11898, 2023. 1, 2, 6, 7, 13, 14, 15, 16, 17, 18, 19
- [35] Hanqing Wang, Wenguan Wang, Wei Liang, Caiming Xiong, and Jianbing Shen. Structured scene memory for vision-language navigation. In *Proceedings of the IEEE/CVF conference on Computer Vision and Pattern Recognition*, pages 8455–8464, 2021. 1
- [36] Peng Wang, An Yang, Rui Men, Junyang Lin, Shuai Bai, Zhikang Li, Jianxin Ma, Chang Zhou, Jingren Zhou, and Hongxia Yang. Ofa: Unifying architectures, tasks, and modalities through a simple sequence-to-sequence learning framework. In *International Conference on Machine Learning*, pages 23318–23340. PMLR, 2022. 7, 18
- [37] Bin Xiao, Haiping Wu, Weijian Xu, Xiyang Dai, Houdong Hu, Yumao Lu, Michael Zeng, Ce Liu, and Lu Yuan. Florence-2: Advancing a unified representation for a variety of vision tasks. In *Proceedings of the IEEE/CVF Conference on Computer Vision and Pattern Recognition*, pages 4818–4829, 2024. 1
- [38] Bin Yan, Yi Jiang, Jiannan Wu, Dong Wang, Ping Luo, Zehuan Yuan, and Huchuan Lu. Universal instance perception as object discovery and retrieval. In *Proceedings of the IEEE/CVF Conference on Computer Vision and Pattern Recognition*, pages 15325–15336, 2023. 1, 2, 6, 14, 15
- [39] An Yang et al. Qwen2 technical report. *arXiv preprint arXiv:2407.10671*, 2024. 5
- [40] Lihe Yang, Bingyi Kang, Zilong Huang, Zhen Zhao, Xiaogang Xu, Jiashi Feng, and Hengshuang Zhao. Depth anything v2. *Advances in Neural Information Processing Systems*, 37:21875–21911, 2024. 5, 19
- [41] Hang Yin, Xiuwei Xu, Linqing Zhao, Ziwei Wang, Jie Zhou, and Jiwen Lu. Unigoal: Towards universal zero-shot goal-oriented navigation. In *Proceedings of the Computer Vision and Pattern Recognition Conference*, pages 19057–19066, 2025. 3
- [42] Naoki Yokoyama, Sehoon Ha, Dhruv Batra, Jiuguang Wang, and Bernadette Bucher. Vlfm: Vision-language frontier maps for zero-shot semantic navigation. In *2024 IEEE International Conference on Robotics and Automation (ICRA)*, pages 42–48. IEEE, 2024. 3
- [43] Licheng Yu, Patrick Poirson, Shan Yang, Alexander C Berg, and Tamara L Berg. Modeling context in referring expressions. In *European Conference on Computer Vision*, pages 69–85. Springer, 2016. 2, 5, 13
- [44] Licheng Yu, Zhe Lin, Xiaohui Shen, Jimei Yang, Xin Lu, Mohit Bansal, and Tamara L Berg. Mattnet: Modular attention network for referring expression comprehension. In *Proceedings of the IEEE Conference on Computer Vision and Pattern Recognition*, pages 1307–1315, 2018. 1, 2, 6, 14
- [45] Yan Zeng, Xinsong Zhang, and Hang Li. Multi-grained vision language pre-training: Aligning texts with visual concepts. In *International Conference on Machine Learning*, pages 25994–26009. PMLR, 2022. 19
- [46] Zhen Zhang, Anran Lin, Chun Wai Wong, Xiangyu Chu, Qi Dou, and KW Samuel Au. Interactive navigation in environments with traversable obstacles using large language and vision-language models. In *2024 IEEE International Conference on Robotics and Automation*, pages 7867–7873. IEEE, 2024. 1, 3

A. Appendix

We used an LLM as a general-purpose writing assistant for minor edits (clarity, grammar, or phrasing) and for generating alternative phrasings of paragraphs we had already drafted.

A.1. Details of VIRO

A.1.1. Input Arguments

We provide the details of VIRO by extracting the program generator prompts. The following functions are available in our framework for reasoning:

- **FIND(object_name='object_name')**: Returns all objects matching the object name which are clearly detectable, excluding non-object entities (e.g., living room, field, wall).
- **LOCATE(object=objects, position='location')**: Returns objects positioned at a specified absolute location, independent of other objects in the 2D space (e.g., 'right', 'at the bottom', 'on left', '9 o clock', 'outmost right', 'top', 'uppermost', 'middle', 'center').
- **ORDER(object=objects, criteria=['left'|'right'|'top'|'bottom'], rank=number)**: Returns the object positioned at the specified rank when sorted only by the given criteria ('left', 'right', 'top', 'bottom'), counting from the end.
- **ABSOLUTE_DEPTH(object=objects, criteria=['front'|'behind'])**: Returns objects from `objects` positioned absolutely closest (front) or farthest (behind) in the 3D space (depth information).
- **SIZE(object=objects, criteria=['big'|'small'])**: Returns objects filtered by relative size only by the given criteria ('big', 'small').
- **PROPERTY(object=objects, value='attribute')**: Filters objects based on their intrinsic attributes (e.g., color and patterns: 'red', 'striped', clothing: 'wearing a blue shirt', states or actions: 'standing', 'sitting', 'turned on', 'open').
- **FIND_DIRECTION(object=objects1, reference_object=objects2, direction=['left'|'right'|'top'|'bottom'])**: Returns objects from `objects1` positioned next to objects in `objects2` only by the given criteria ('left', 'right', 'top', 'bottom').
- **FIND_NEAR(object=objects1, reference_object=objects2)**: Returns objects from `objects1` that are spatially close to any object in `objects2`.
- **FIND_INSIDE(object=objects1, reference_object=objects2)**: Returns objects from `objects1` that are strictly inside the reference object `objects2`.
- **RELATIVE_DEPTH(object=objects1, reference_object=objects2, criteria=['front'|'behind'])**: Returns objects from `objects1` positioned in depth relative to objects in `objects2` only by the given criteria ('front', 'behind').
- **RESULT(object=answer_object)**: Pre-processes the final selected object to the final answer form.

A.1.2. Verification Module

Attribute Operator. We use the `PROPERTY` operator to filter visual attributes using the CLIP and GroundingDINO-T model. CLIP has varying thresholds depending on the given image, which makes filtering based solely on similarity scores challenging. To improve the filtering process, we first apply a softmax transformation to the CLIP similarity scores of the candidate regions from the OVD. We then integrate GroundingDINO-T scores into the filtering process, combining them with the softmax CLIP scores via a weighted sum. Finally, we set an adaptive threshold based on the number of candidates from `FIND` operator.

Relative Spatial Operators. Relative spatial operators take at least two arguments: `object` and `reference_object`. The `reference_object` serves as the spatial standard, and the `object` denotes the entity whose position is specified relative to this reference. As discussed in Section 3.2.1, we use logical verification in `RELATIVE_DEPTH`, similar to `FIND_DIRECTION`, but with the relative depth values 'front' or 'behind'. Additionally, in `FIND_INSIDE`, if there is no intersection area between the `object` and `reference_object`, the proposal is rejected.

A.1.3. Adaptive Threshold

To compute the filtering score $S(l|I_j)$ in equation (2), for each candidate region I_j with label l , we leverage a pre-trained VLM trained with contrastive loss, such as CLIP. CLIP is designed to align visual and textual representations in a shared embedding space, enabling effective discrimination between semantically relevant (positive) and irrelevant (negative) pairs. However, one of the main challenges when using CLIP for verification is its inherent bias toward labels that appear frequently in its training data. Labels like 'person' or 'car' typically receive higher confidence scores compared to more specialized or rare objects, making a fixed threshold inappropriate for fair evaluation across different object categories. To address this label-specific bias, we implement an adaptive thresholding mechanism that calibrates the decision boundary for each target

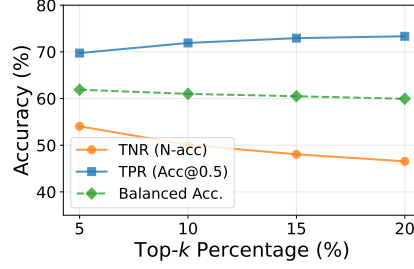


Figure A1. Analysis of k adaptive threshold which illustrates the trade-off between TPR and TNR.

label individually. We utilize ImageNet as an auxiliary calibration dataset, computing verification scores for a representative sample of images containing various object categories.

We collect 5 images per class in ImageNet (a total of 5,000 images) and use GroundingDINO to crop out only the relevant class objects (denoted as D_A). This process helps minimize bias from background elements, where many images contain a person even when the target class is not ‘person’. For each target label l , we analyze the distribution of verification scores $S(l|I)$ across this preprocessed dataset to determine CLIP’s typical confidence range for that specific category.

The calibration process employs a top- k selection strategy to determine the appropriate threshold δ_l . Specifically, we rank all verification scores computed on the auxiliary dataset for target label l where $d \in D_A$, and the score is defined as:

$$S(l|d_i) = \frac{1}{K} \sum_{k=1}^K \frac{\exp(\text{sim}(d_i, l)/\tau)}{\exp(\text{sim}(d_i, l)/\tau) + \exp(\text{sim}(d_i, c_k)/\tau)}. \quad (5)$$

The set of verification scores for the entire dataset is represented as:

$$S(l|D_A) = \{S(l|d_1), S(l|d_2), \dots, S(l|d_n)\}, \quad (6)$$

where n is the number of auxiliary dataset. The threshold δ_l selects the top- $k\%$ highest scoring samples, where k is a hyperparameter (typically set as 10). This strategy effectively captures the performance level that CLIP consistently achieves for high-confidence predictions of the target category, providing a data-driven threshold that reflects CLIP’s inherent capability for that specific label.

We also investigate the sensitivity of our pipeline to k . As shown in Figure A1, VIRO’s performance remains highly robust to changes in the Top- k percentage. Although a slight increase in TPR is observed with more candidates (as the ground-truth box is more likely to be included), the overall Balanced Accuracy stays stable across different values of k .

A.1.4. Justification for Neuro-symbolic Verification

VIRO addresses two fundamental limitations in existing approaches: *unreliable verification* and *cascading errors*. First, free-form Python approaches rely on LLM-generated code for verification (e.g., `if` blocks), which is not explicitly enforced and thus prone to being incorrectly generated or omitted. In contrast, VIRO restricts program generation to a pre-defined set of verifiable primitives. Furthermore, methods like NAVER perform verification only after all reasoning steps, making them prone to cascading errors: inevitable false positives from open-vocabulary detectors propagate through intermediate reasoning steps and corrupt final predictions. In contrast, VIRO’s operator-level verification ensures high-precision grounding by filtering out incorrect candidates.

A.2. Program Validator

The Program Validator serves as a safeguard against errors in LLM-generated programs. Its primary purpose is to detect syntactic, structural, and logical mistakes before program execution, and to provide structured feedback tailored to the specific type of error. Since LLM outputs are not guaranteed to be flawless, the validator detects invalid programs at pre-execution time and provides feedback that guides the LLM to regenerate a correct program.

A valid program must follow a simple and strict format: each line is written as `VAR = OP (ARG=..., ...)` and executed sequentially in order, while the program always terminates with a line that must take the form `FINAL_RESULT = RESULT (object=VAR)`. Given this constrained design, the validator enforces the following properties:

- **Syntax enforcement:** all lines except the last must take the form `VAR = OP (ARG=..., ...)`, and the last line must take the form `FINAL_RESULT = RESULT (object=VAR)`.

- **Variable tracking:** at line t , only variables defined in lines $1, \dots, t - 1$ may be referenced, and redefinition of an existing variable is disallowed to prevent overwriting outputs from earlier steps.
- **Argument typing:** arguments are checked for valid type (variable, string, or number). Certain arguments have additional constraints, e.g., `rank` must be a positive integer and `criteria` must be chosen from a predefined set (e.g., `left`, `right`, `top`, `bottom`).
- **Operator constraints:** each operator must belong to the predefined functions (e.g., `FIND`, `PROPERTY`), and each function must include all of its required arguments.
- **Output format:** the program must end with a single line in the form `FINAL_RESULT = RESULT(object=VAR)`, and no other `RESULT` may appear earlier in the program.

Through these checks, the Program Validator acts as a reliable feedback mechanism, reducing execution errors caused by incorrect code generated by the LLM. Both our method and ViperGPT [34] use programs generated by the LLM prior to execution, but the scope of validation differs fundamentally. ViperGPT only ensures that the generated code is syntactically valid Python code, which allows issues such as undefined variables, incorrect argument types, or missing required arguments to pass through unnoticed until runtime. In contrast, our validator applies strict structural and semantic checks before execution, ensuring correct format, valid variables, and a proper output statement. These checks reduce execution errors and provide targeted feedback for correction.

A.3. Experimental Setup

A.3.1. Datasets

RefCOCO+/g. RefCOCO [43] primarily targets location-based expressions, while RefCOCO+ [43] focuses on attribute-based descriptions by prohibiting the use of absolute location words. RefCOCOg [26], in contrast, contains longer and more complex expressions, often combining both spatial relations and attributes. For RefCOCO and RefCOCO+, results are reported separately on two test splits: TestA, where the referent is a person, and TestB, where the referent is a non-person object, highlighting object-centric grounding. For RefCOCOg, results are reported on the standard single test split. All of these benchmarks are built upon the MSCOCO [23] image dataset.

gRefCOCO no-target split. gRefCOCO [11, 24] is a referring expression dataset that explicitly includes no-target queries, allowing evaluation of systems that must either localize the referred region or abstain when no valid target exists. To avoid trivial negatives, no-target expressions are constrained to be contextually related to the image, and annotators may reuse deceptive expressions from the same split when needed.

RefAdv. RefAdv [1] is an out-of-distribution (OOD) adversarial test set derived from Ref-Hard, the structure-dependent subset of RefCOCOg, designed to evaluate whether referring expression models truly leverage syntactic structure rather than rely on lexical cues. It reveals models’ lack of syntactic understanding and limited generalization, even for those that perform well on the original RefCOCOg benchmark.

RefEgo. RefEgo [18] is a video-based referring expression comprehension (REC) dataset built upon first-person videos from the Ego4D [8], designed to evaluate models’ ability to localize objects described in natural language under realistic conditions. The dataset contains clips, which are selected to feature rapid egocentric camera motion and multiple similar objects, and some include frames where the target object is absent, requiring models to detect no-target situations. Unlike prior REC datasets built from web-curated images, RefEgo focuses on testing language–vision grounding and generalization in real-world environments.

A.3.2. Evaluation Metrics

We assess both *no-target robustness* and standard REC accuracy, which jointly require addressing localization and classification. Following a binary classification view, we define outcomes based on the confusion matrix: **True Positive (TP)**: a target is present and the model correctly localizes it (Intersection-over-Union (IoU) > 0.5); **True Negative (TN)**: target is absent and the model correctly predicts its absence; **False Positive (FP)**: target is absent but the model incorrectly outputs a bounding box; and **False Negative (FN)**: a target is present but the model either predicts ‘no-target’ or localizes it incorrectly (IoU < 0.5).

A.3.3. Baseline Details

Fully supervised REC baselines are trained with full annotations on RefCOCO+/g. GREC [11] further incorporates the gRefCOCO no-target dataset to address target-absent cases. By contrast, Qwen2.5-VL-72B-AWQ [2] is evaluated without fine-tuning on gRefCOCO. To enable no-target prediction, we append a negative instruction to its prompt, e.g., “if there is no object, return []”, thereby leveraging its inherent reasoning capability. The full prompt for Qwen2.5-VL is as follows: Detect

{description} in the image. Return a JSON list of bounding boxes as [x1, y1, x2, y2] in pixel coordinates relative to the input image. If there is no object, return [].

Proposal-based REC first parses the referring expression to isolate key linguistic components before matching them against pre-generated object proposals. **ReCLIP** [33] employs a syntactic parser to extract noun chunks, while **GroundVLP** [31] utilizes a traditional NLP toolbox to identify the main object. More recent approaches leverage the advanced capabilities of Large Language Models (LLMs) for this task; **SS-CLIP/SS-FLAVA** [10], two variants of the method in [10], use an LLM to parse the main object from the query. After this initial parsing stage, each method employs its unique mechanism to map the extracted components to the most relevant regions in given detected proposals from MAttNet [44]. These are architecturally constrained to a rich pool of candidate regions by Faster RCNN, making a direct comparison on target-absent task unfair.

Compositional reasoning REC parses complex queries into explicit programs. By generating and then executing these programs, they transparently handle multi-step compositional logic to derive the final result. We compare our approach with state-of-the-art methods in this domain, including **ViperGPT** [34], **HYDRA** [16], and **NAVER** [3], to benchmark its compositional reasoning capabilities.

A.4. Standard REC Accuracy Under Forced Prediction

Our framework is evaluated under a target-present assumption, wherein each query is guaranteed to have a corresponding target in the image. In this setting, our approach achieves high accuracy on standard benchmarks, as summarized in Table A1.

Table A1. Comparison of REC methods on standard benchmarks in terms of TPR (Acc@0.5), under a forced prediction setting.

Method	RefCOCO			RefCOCO+			RefCOCOg	
	Val	TestA	TestB	Val	TestA	TestB	Val	Test
Fully Supervised REC								
Qwen2.5-VL-72B [2]	92.7	94.6	89.7	88.9	92.2	83.7	89.9	90.3
GREC-MDETR-R101 [15]	86.8	89.6	81.4	79.5	84.1	70.6	81.6	80.9
GREC-UNINEXT-R50 [38]	89.7	91.5	86.9	79.8	85.2	72.8	84.0	84.3
Proposal-based REC								
ReCLIP [33]	45.8	47.0	45.2	45.3	48.5	42.7	57.0	56.2
SS-CLIP [10]	60.6	66.5	54.9	55.5	62.6	45.7	59.9	59.9
SS-FLAVA [10]	52.5	52.7	52.9	50.8	53.4	47.6	61.3	60.9
GroundVLP [31]	52.6	61.3	43.5	56.4	64.8	47.4	64.3	63.5
Detector-based REC								
GLIP-L [21]	47.5	52.6	41.8	44.1	48.6	39.8	51.9	52.6
GroundingDINO-T [25]	50.4	57.2	43.2	51.4	57.6	45.8	60.4	59.5
Compositional Reasoning REC with GLIP								
ViperGPT [34]	66.9	72.0	59.9	59.6	65.7	63.0	69.3	69.6
HYDRA [16]	68.0	73.1	62.5	55.8	60.6	50.6	67.2	67.6
NAVER [3]	69.6	73.4	64.4	59.0	62.7	56.4	70.7	70.0
VIRO (Ours)	71.4	75.7	63.8	59.3	66.2	51.3	70.6	71.5
Compositional Reasoning REC with GroundingDINO								
ViperGPT [34]	62.2	66.7	54.6	55.4	61.7	50.4	66.0	65.7
HYDRA [16]	62.0	62.8	62.4	55.0	58.4	51.6	66.4	67.1
NAVER [3]	61.1	64.2	58.2	56.4	60.1	51.8	68.4	68.4
GDINO-FLORA [‡] [4]	73.7	78.5	67.8	63.2	71.6	53.5	72.5	72.1
VIRO (Ours)	71.4	75.0	64.4	59.5	65.8	50.1	69.6	70.3

[‡] Official code has not been released as of September 25, 2025.

A.5. Handling No-Target Cases and Errors in Baselines

This section defines how we count no-target predictions and attribute errors for the baselines evaluated in our study. For **detector-based baselines**, if the detector returns no bounding boxes for the query, we label the prediction as no-target (correct). For **compositional-reasoning REC** baselines, prior implementations do not explicitly consider no-target cases; we therefore specify our handling of no-target outcomes and errors. Specifically, if the framework’s final output is the empty set, we count the prediction as *no-target (correct)*. Further method-specific details are provided below.

ViperGPT [34]. In our evaluation of ViperGPT, an instance is classified as a no-target if the final code execution resulted in an empty list. Errors are identified when the `exec(compile(code, 'Codex', 'exec'), globals())` call returned `None`, which typically signifies a failure during code execution. ViperGPT’s instructions enforce a fallback that retrieves the entire image when an object is not detected (e.g., when `len(object)==0`). This design choice creates ambiguity in identifying no-targets case. While likely intended to prevent downstream Python errors, this execution-safety behavior makes it difficult to distinguish a true ‘no object found’ scenario. We therefore adopt a conservative rule: treat only an empty final result as no-target, and treat `None` as error.

HYDRA [16]. For HYDRA, we adapt a strict criterion for no-target cases: we label no-target (correct) only when the number of detected main objects or relation-forming objects is exactly zero (i.e., `len(...)==0`). Conversely, any case with `len(...)` ≥ 1 is classified as an error. While it could potentially represent a no-target scenario (e.g., the model detected objects but failed to establish the queried relationship), it is not possible to definitively confirm this. Therefore, to maintain a conservative count of true no-target instances, we opt to classify these ambiguous cases as errors.

NAVER [3]. The NAVER pipeline operates through four distinct stages, each equipped with a self-correction mechanism: Perception, Logic Generation, Logic Reasoning, and Logic Answering. If the Perception stage fails to produce region proposals, it retries with a lower object detection threshold. In the Logic Generation stage, a failure prompts the LLM to retry the generation process. If the Logic Reasoning stage encounters a code error or yields no-target candidates, the pipeline reverts to the Logic Generation stage to create a new logical program. Finally, in the Answering stage, a Multimodal Large Language Model (MLLM)—specifically InternVL2-8B [5]—is prompted with the question, “Does the object meet the query?” If the MLLM answers ‘no,’ this stage is also retried.

After a maximum of five retry attempts across the pipeline, a query is classified as a no-target under one of three conditions: (i) perception failure (no detection), (ii) logic reasoning fails to establish the required relations (e.g., `contains`, `inside`, `is`), and (iii) the MLLM consistently answers ‘no,’ in answering state, indicating that no identified object satisfies the query.

Based on our implementation of the official code (at the time of our experiments), we observe that the vast majority of processing errors occur during the Logic Reasoning stage, specifically during the translation to or execution of the Probabilistic Prolog program. Further analysis of NAVER’s no-target cases is provided in Appendix A.6.3.

A.6. Detailed Experimental Results

We provide full benchmark results and baseline details across all evaluation splits for completeness.

A.6.1. Baseline Implementation for No-Target Cases

We evaluate our model’s ability to handle negative cases where the target is not present in the image. The results on the gRefCOCO no-target split are shown in Table A2.

Table A2. Quantitative evaluation of no-target robustness on the gRefCOCO no-target split, reported as TNR (N-acc) (%).

Method	Val	TestA	TestB
<i>Fully Supervised REC</i>			
GREC-MDETR-R101 [15]	36.3	34.5	31.0
GREC-UNINEXT-R50 [38]	50.6	49.3	48.2
<i>Detector-based REC</i>			
GLIP-L [21]	14.8	21.7	18.2
GroundingDINO-T [25]	2.0	22.8	16.0
<i>Compositional Reasoning REC with GLIP</i>			
ViperGPT [34]	0.3	0.1	0.1
HYDRA [16]	7.2	6.3	6.1
NAVER [3]	14.9	13.9	13.0
VIRO (Ours)	56.7	50.1	53.2
<i>Compositional Reasoning REC with GroundingDINO</i>			
ViperGPT [34]	0.3	0.2	0.1
HYDRA [16]	8.6	7.5	7.0
NAVER [3]	3.0	3.4	1.8
VIRO (Ours)	56.5	50.2	52.9

A.6.2. Baseline Implementation for Standard REC Benchmarks

The detailed results for the RefCOCO, RefCOCO+, and RefCOCOg datasets are provided in Table A3, Table A4, and Table A5, respectively.

Table A3. Quantitative results on the RefCOCO dataset. Accuracy (%) is evaluated under two conditions: including all predictions (Inc.↑) and excluding model failure cases (Exc.↑). FR denotes the overall Failure Rate (%).

Method	Val			TestA			TestB		
	FR ↓	Exc.↑	Inc.↑	FR ↓	Exc.↑	Inc.↑	FR ↓	Exc.↑	Inc.↑
Detector-based REC									
GLIP-L [21]	0.00	47.5	47.5	0.00	52.6	52.6	0.00	41.8	41.8
GroundingDINO-T [25]	0.00	50.4	50.4	0.00	57.2	57.2	0.00	43.2	43.2
Compositional Reasoning REC with GLIP									
ViperGPT [34]	4.12	66.9	64.1	3.32	72.0	69.6	5.16	59.9	56.8
HYDRA [16]	19.60	68.0	54.7	17.27	73.1	60.5	24.14	62.5	47.4
NAVER [3]	17.97	69.6	57.1	14.85	73.4	62.5	20.71	64.4	51.1
VIRO (Ours)	0.09	68.1	68.1	0.07	72.8	72.8	0.14	60.6	60.5
Compositional Reasoning REC with GroundingDINO									
ViperGPT [34]	3.90	62.2	59.8	3.45	66.7	64.4	4.71	54.6	52.0
HYDRA [16]	26.13	62.0	45.8	28.46	62.8	44.9	34.6	62.4	40.8
NAVER [3]	8.77	61.1	55.7	6.01	64.2	60.3	10.70	58.2	52.0
VIRO (Ours)	0.09	68.2	68.1	0.07	71.9	71.9	0.14	60.8	60.8

Table A4. Quantitative results on the RefCOCO+ dataset. Accuracy (%) is evaluated under two conditions: including all predictions (Inc.↑) and excluding model failure cases (Exc.↑). FR denotes the overall Failure Rate (%).

Method	Val			TestA			TestB		
	FR ↓	Exc.↑	Inc.↑	FR ↓	Exc.↑	Inc.↑	FR ↓	Exc.↑	Inc.↑
Detector-based REC									
GLIP-L [21]	0.00	44.1	44.1	0.00	48.6	48.6	0.00	39.8	39.8
GroundingDINO-T [25]	0.00	51.4	51.4	0.00	57.6	57.6	0.00	45.8	45.8
Compositional Reasoning REC with GLIP									
ViperGPT [34]	6.97	59.6	55.4	3.28	65.7	63.6	6.73	53.0	49.4
HYDRA [16]	24.40	55.8	42.2	17.06	60.6	50.3	30.91	50.6	35.0
NAVER [3]	26.44	59.0	43.4	14.67	62.7	53.5	33.59	56.4	37.5
VIRO (Ours)	0.08	56.1	56.0	0.07	63.7	63.7	0.12	47.0	47.0
Compositional Reasoning REC with GroundingDINO									
ViperGPT [34]	6.71	55.4	51.7	6.83	61.7	57.5	6.46	50.4	47.1
HYDRA [16]	33.16	55.0	36.8	35.96	58.4	37.4	29.72	51.6	36.3
NAVER [3]	14.50	56.4	48.2	7.39	60.1	55.7	20.82	51.8	41.0
VIRO (Ours)	0.08	56.6	56.5	0.00	63.3	63.3	0.12	46.2	46.2

A.6.3. Analysis of NAVER

The Perception, Logic Reasoning, and Logic Answering modules in NAVER invoke self-correction when no valid target is found, effectively forcing an object prediction. To evaluate performance on the no-target split, we disable this behavior in all three modules and adopt an *early-exit* policy that stops the pipeline when “no-target” is detected. We report TNR on the gRefCOCO testA no-target set, and TPR on the RefCOCO testA set. As shown in Table A6, disabling self-correction improves TNR but at the cost of TPR. The module-wise distribution of early exits—indicating which component identifies the target’s absence—is summarized in Table A7. This analysis is intended to isolate no-target behavior and does not reflect the default official setting.

Table A5. Quantitative results on the RefCOCOg dataset. Accuracy (%) is evaluated under two conditions: including all predictions (Inc.↑) and excluding model failure cases (Exc.↑). FR denotes the overall Failure Rate (%).

Method	Val			Test		
	FR ↓	Exc.↑	Inc.↑	FR ↓	Exc.↑	Inc.↑
Detector-based REC						
GLIP-L [21]	0.00	51.9	51.9	0.00	52.6	52.6
GroundingDINO-T [25]	0.00	60.4	60.4	0.00	59.5	59.5
Compositional Reasoning REC with GLIP						
ViperGPT [34]	7.40	69.3	64.2	6.31	69.6	65.2
HYDRA [16]	23.98	67.2	51.1	21.44	67.6	53.1
NAVER [3]	28.44	70.7	50.6	25.90	70.0	51.9
VIRO (Ours)	0.28	66.2	66.0	0.38	67.0	66.8
Compositional Reasoning REC with GroundingDINO						
ViperGPT [34]	6.55	66.0	61.7	6.03	65.7	61.7
HYDRA [16]	34.07	66.4	43.8	32.37	67.1	45.4
NAVER [3]	38.50	68.4	42.1	9.74	68.4	55.8
VIRO (Ours)	0.24	66.2	66.0	0.38	66.6	66.3

Table A6. Impact of the self-correction on the NAVER framework. Performance is evaluated on gRefCOCO no-target TestA (TNR) and RefCOCO TestA (TPR) datasets.

Method	Balanced Acc ↑	TNR _(gRef) ↑	TPR _(Ref) ↑
NAVER w/ self-correction	33.8	3.4	64.2
NAVER w/o self-correction	63.2	71.6	54.8

Table A7. Frequency (%) of early exits per NAVER module contributing to TNR on the gRefCOCO no-target TestA split.

Module	Frequency (%)
Perception	67.8
Logic Reasoning	11.7
Logic Answering	20.5

A.6.4. Results on RefAdv dataset

To further evaluate the robustness of VIRO to linguistic perturbations, we analyze performance on the RefAdv benchmark, which introduces adversarially reordered referring expressions designed to test whether models rely on true syntactic understanding rather than superficial lexical cues. As shown in Table A8, VIRO achieves 64.2% Exc. and 63.8% Inc. accuracy on RefAdv, substantially outperforming prior compositional baselines, whose accuracy drops sharply due to frequent program-generation or execution failures.

A.6.5. Results on RefEgo validation set

In this section, we provide a detailed performance analysis on the RefEgo validation set in Table A9, extending the test set results presented in the main paper. While VIRO is not explicitly trained on egocentric video data, it significantly outperforms other off-the-shelf REC models such as OFA and MDETR. Notably, VIRO achieves 49.6% in Acc@0.5+n, demonstrating its strong zero-shot transferability in complex grounding scenarios without any task-specific fine-tuning.

A.7. Runtime Analysis with LLM backbones

We analyze the end-to-end latency of VIRO by decomposing the per-query runtime into two distinct stages: *pre-execution* and *execution*. As shown in Table A10, API-based models significantly reduce pre-execution overhead while maintaining competitive TPR. While a large-scale local LLM (Qwen2.5-72B-Instruct-AWQ) requires 12.21s for pre-execution, API-based acceleration via GPT-4o reduces this latency to 1.06s—a nearly 11.5× speedup—while even achieving higher TPR (72.3%). Consequently, the total runtime becomes dominated solely by the execution stage (fixed at 0.71s), rather than the reasoning

Table A8. Quantitative results with GroundingDINO on the RefAdv dataset. Accuracy (%) is evaluated under two conditions: including all dataset (Inc.↑) and excluding model failure cases (Exc.↑). FR denotes the overall Failure Rate (%).

Method	Test		
	FR ↓	Exc. ↑	Inc. ↑
<i>Detector-based REC</i>			
GLIP-L [21]	0.00	55.7	55.7
GroundingDINO-T [25]	0.00	60.5	60.5
<i>Compositional Reasoning REC</i>			
ViperGPT [34]	11.47	64.8	57.3
HYDRA [16]	36.61	65.8	41.7
NAVER [3]	13.23	64.0	55.5
VIRO (Ours)	0.59	64.2	63.8

Table A9. Comparison of video-based REC performance on the RefEgo validation set.

Method	All Frames		Target-present
	mSTIoU	Acc@0.5+n	TPR (Acc@0.5)
<i>Fully Supervised with RefEgo</i>			
MDETR+BH [18]	37.9	51.9	52.9
<i>Off-the-shelf RefCOCOg model</i>			
OFA [36]	16.9	30.8	29.6
MDETR [15]	17.4	28.3	25.2
<i>Compositional Reasoning REC with GroundingDINO</i>			
ViperGPT [34]	9.5	16.4	14.3
VIRO (Ours)	23.0	49.6	33.9

overhead. This efficiency is a direct consequence of VIRO’s decoupled design, which enables flexible backbone selection to optimize latency-accuracy trade-offs.

Table A10. Pre-execution (Pre-exec.) runtime and accuracy comparison across different LLM backbones on RefCOCO testA. **The execution stage maintains a constant latency of 0.71s across all models**, reflecting VIRO’s decoupled architecture.

LLM Backbone	Pre-exec. (s)	TPR (%)
Llama3.1-8B-Instruct (Local)	2.07	66.3
Qwen2.5-72B-Instruct-AWQ (Local)	12.21	71.9
GPT-4o mini (API)	1.37	69.1
GPT-4o (API)	1.06	72.3

A.8. Models Used in Compositional Baselines and VRAM Usage

Table A11 details the pre-trained vision-language components employed by each compositional baseline and their corresponding peak VRAM consumption, measured on an NVIDIA RTX A6000 (48GB). To ensure a focused comparison on the vision-language backbone efficiency, the reported memory excludes the VRAM occupied by the LLM itself.

Existing compositional baselines typically rely on heavy Multimodal LLMs (MLLMs), which incur significant memory and computational overhead. To avoid such overhead, VIRO is designed to operate without a MLLM, instead utilizing a more lightweight verification process. Furthermore, unlike NAVER, which requires an additional SegmentAnything [17] model, VIRO maintains a minimal set of components, requiring only 9.7GB of VRAM. Note that VRAM usage among baselines may vary depending on specific model-loading strategies, such as full pre-loading versus modular execution.

Table A11. Comparison of visual-language components and peak VRAM usage. Memory is measured during inference, excluding the LLM backbone.

	ViperGPT [34]	HYDRA [16]	NAVER [3]	VIRO (Ours)
Multimodal Encoder	X-VLM [45]	X-VLM [45]	X-VLM [45]	CLIP [28]
Open-set Detector	GDINO-T [25]	GDINO-T [25]	GDINO-T [25]	GDINO-T [25]
Depth Estimator	DPT-Large [29]	DPT-Large [29]	DepthAnythingV2 [40]	DepthAnythingV2 [40]
Multimodal LLM	BLIP-2 [20]	BLIP-2 [20]	InternVL2 [5]	N/A
Mask Generator	N/A	N/A	SegmentAnything [17]	N/A
VLM Memory Load	35.0 GB	21.8GB	29.9 GB	9.7 GB

A.9. Further Ablation Analysis

A.9.1. LLM Ablation Studies

To demonstrate that VIRO’s performance stems from its architectural design rather than a specific LLM, we evaluate its robustness and scalability across various backbones, ranging from the Llama-3.1-8B [7] to the GPT-4o/mini [13].

First, we conduct an ablation study in which we replace the primary LLM backbone used in our main experiments with Llama-3.1-8B-Instruct [7], while keeping all other components and hyperparameters unchanged. The results, presented in Table A12, show that VIRO achieves a lower program-generation failure rate and maintains strong performance with Llama-3.1-8B. In contrast, ViperGPT and NAVER exhibit very high failure rates, which leads to substantially reduced Inc. TPR. We omit the results for HYDRA with Llama-3.1-8B-Instruct, as the model failed on nearly all queries; specifically, it struggled to adhere to HYDRA’s iterative generation instructions, where even a minor formatting error caused the entire execution pipeline to collapse.

Table A12. Performance comparison on standard REC benchmarks using Llama3.1-8B-Instruct [7] as an alternative LLM backbone. We report results on the testA splits of RefCOCO/+ and the test split of RefCOCOg. Accuracy is measured both including (Inc.↑) and excluding (Exc.↑) failure cases. The failure rate (%) is reported for RefCOCOg.

Method	Failure Rate ↓	RefCOCO		RefCOCO+		RefCOCOg	
		Exc. ↑	Inc. ↑	Exc. ↑	Inc. ↑	Exc. ↑	Inc. ↑
<i>Detector-based REC</i>							
GLIP-L [21]	0.00	52.6	52.6	48.6	48.6	52.6	52.6
GroundingDINO-T [25]	0.00	57.2	57.2	57.6	57.6	59.5	59.5
<i>Compositional Reasoning REC with GLIP</i>							
ViperGPT [34]	40.09	65.1	48.4	53.2	41.3	57.6	35.1
NAVER [3]	70.15	72.3	32.4	65.1	28.6	69.6	20.8
VIRO (Ours)	0.34	68.2	68.2	56.6	56.6	61.4	61.4
<i>Compositional Reasoning REC with GroundingDINO</i>							
ViperGPT [34]	41.82	59.1	43.7	48.0	37.5	52.1	31.7
NAVER [3]	54.84	61.3	43.1	59.7	40.9	64.7	29.2
VIRO (Ours)	0.34	66.3	66.3	55.3	55.3	60.9	60.9

We further explore the scalability of our framework using GPT-4o and GPT-4o mini, while simultaneously clarifying the performance gap observed with the official NAVER results. As shown in Table A13, the high performance of NAVER (91.7%) stems from their use of a GroundingDINO-B detector fine-tuned on RefCOCO. To ensure a strictly zero-shot evaluation, we instead utilize GroundingDINO-T, which has not been exposed to the RefCOCO training set. Notably, when evaluated using the same zero-shot detector, VIRO consistently outperforms NAVER, confirming that our framework provides stronger zero-shot performance.

A.9.2. Early-exit Mechanism.

As shown in Table A14, incorporating the early-exit reduces the average latency focusing on the program execution phase to 0.52 seconds per query on the gRefCOCO no-target testA split. Since operators run sequentially, unmet intermediate conditions trigger immediate termination of the execution pipeline. For example, in the query ”an elephant to the left of a

Table A13. Comparison of performance on the RefCOCO testA split using GPT-4o and GPT-4o mini. For a fair comparison, all methods are evaluated in a zero-shot setting except for the official NAVER entry using a fine-tuned detector.

Method	LLM	Detector	Acc@0.5
NAVER (Official)	GPT-4o-mini	GroundingDINO-B*	91.7
<i>Fair Comparison: Zero-shot Setting</i>			
NAVER (Official)	GPT-4o-mini	GroundingDINO-T	64.9
VIRO (Ours)	GPT-4o-mini	GroundingDINO-T	69.1
VIRO (Ours)	GPT-4o	GroundingDINO-T	72.3

*Fine-tuned on the RefCOCO training set.

man,” the program exits as soon as the elephant is not found, thereby pruning redundant downstream visual operations. This mechanism effectively boosts throughput in scenarios where no-target cases are frequent.

Table A14. Ablation study on the early-exit mechanism. Latency and FPS are measured solely for the program execution stage, evaluated on the gRefCOCO no-target testA split.

Early-exit	Latency ↓	FPS ↑
Enabled	0.52	1.92
Disabled	0.58	1.79

A.10. Extension to Visual Question Answering via GQA

As a preliminary extension beyond REC, we adapt VIRO to the GQA dataset [12], a compositional VQA benchmark, as shown in Table A15. For a fair comparison, we utilize the same backbone models (BLIP-2, GLIP, and GPT-3.5-turbo) following the setup in HYDRA. For this task, we introduce two new operators: ASK for QA generation and CROP_DIRECTION for spatial focusing. This adaptation is implemented modularly by (i) defining the corresponding Python logic and (ii) registering the operators in the in-context prompt, allowing VIRO to support this task without retraining.

Table A15. Comparison of accuracy (%) on the GQA dataset.

Method	Acc
<i>Trained RL Controller</i>	
HYDRA (Official)	47.9
<i>Zero-shot Setting</i>	
ViperGPT (Official)	37.9
VIRO (Ours)	45.4

A.11. Qualitative Analysis

We present qualitative examples from RefCOCO validation set. Figure A2 demonstrates VIRO’s ability to suppress false positives (FPs) from open-vocabulary detectors via CLIP-based verification, compared against previous REC methods.

A.12. VIRO Execution Examples

Figures A3, A4, and A5 show our program’s execution process.

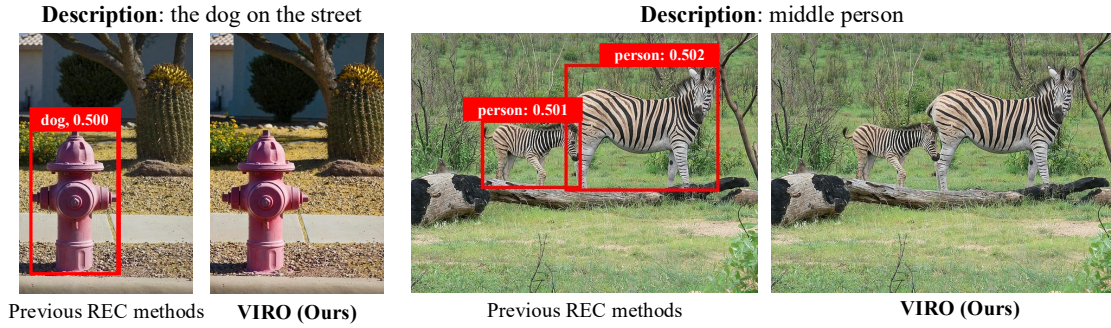


Figure A2. RefCOCO validation examples for false-positive suppression. Prior REC methods (left) yield spurious detections (red), whereas VIRO (right) rejects them via CLIP-based verification.

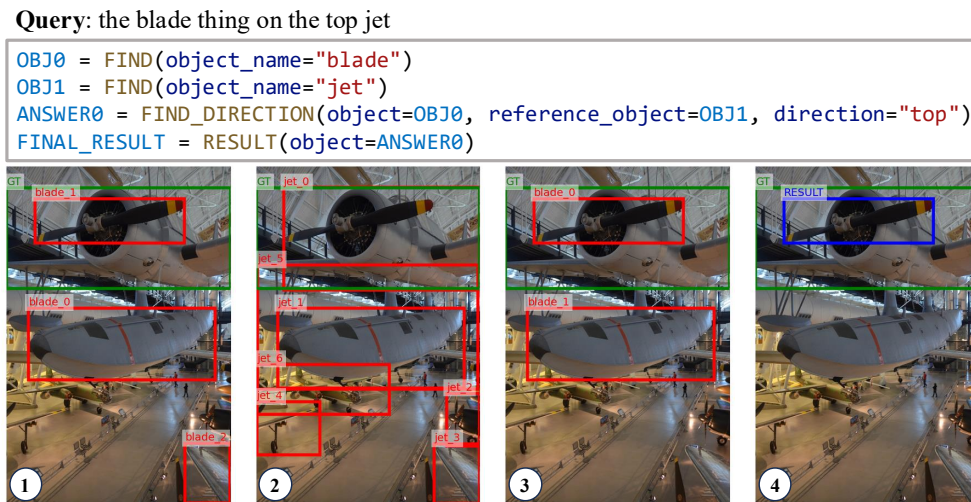


Figure A3. Program generated for the query “the blade thing on the top jet” (top), along with its sequential execution from step 1 to step 4 (bottom).

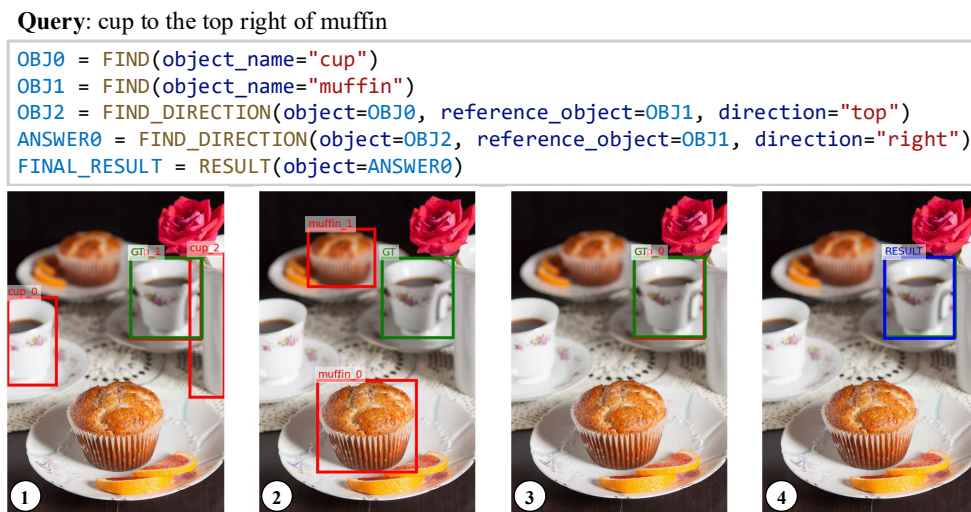


Figure A4. Program generated for the query “cup to the top right of muffin” (top), along with its sequential execution from step 1 to step 4 (bottom).

Query: man at head of table white shirt closest

```
OBJ0 = FIND(object_name="man")
OBJ1 = PROPERTY(object=OBJ0, value="wearing white shirt")
OBJ2 = FIND(object_name="table")
OBJ3 = FIND_DIRECTION(object=OBJ1, reference_object=OBJ2, direction="top")
ANSWER0 = ABSOLUTE_DEPTH(object=OBJ3, criteria="front")
FINAL_RESULT = RESULT(object=ANSWER0)
```

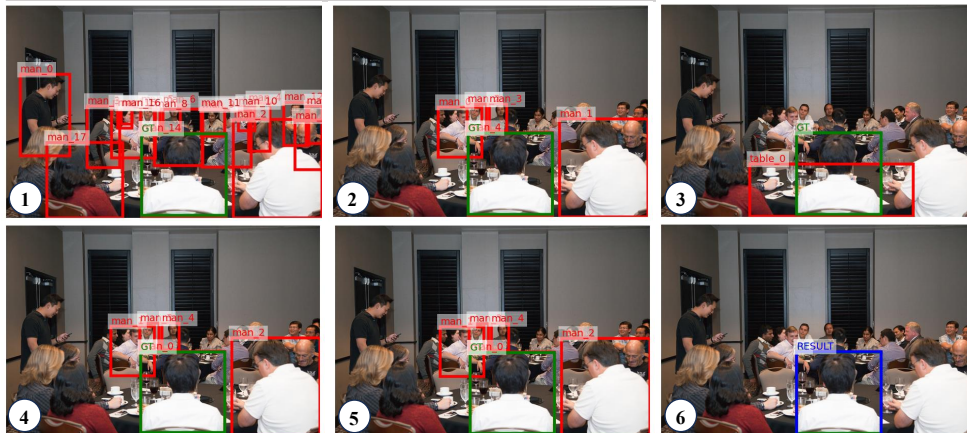


Figure A5. Program generated for the query “man at head of table white shirt closest” (top), along with its sequential execution from step 1 to step 6 (bottom).